

Matched interface and boundary (MIB) method for the vibration analysis of plates

S. N. Yu¹, Y. Xiang² and G. W. Wei^{1, 3, *, †}

¹*Department of Mathematics, Michigan State University, East Lansing, MI 48824, U.S.A.*

²*School of Engineering, University of Western Sydney, Penrith South DC, NSW 1797, Australia*

³*Department of Electrical and Computer Engineering, Michigan State University, East Lansing, MI 48824, U.S.A.*

SUMMARY

This paper proposes a novel approach, the matched interface and boundary (MIB) method, for the vibration analysis of rectangular plates with simply supported, clamped and free edges, and their arbitrary combinations. In previous work, the MIB method was developed for three-dimensional elliptic equations with arbitrarily complex material interfaces and geometric shapes. The present work generalizes the MIB method for eigenvalue problems in structural analysis with complex boundary conditions. The MIB method utilizes both uniform and non-uniform Cartesian grids. Fictitious values are utilized to facilitate the central finite difference schemes throughout the entire computational domain. Boundary conditions are enforced with fictitious values—a common practice used in the previous discrete singular convolution algorithm. An essential idea of the MIB method is to repeatedly use the boundary conditions to achieve arbitrarily high-order accuracy. A new feature in the proposed approach is the implementation of the cross derivatives in the free boundary conditions. The proposed method has a banded matrix. Nine different plates, particularly those with free edges and free corners, are employed to validate the proposed method. The performance of the proposed method is compared with that of other established methods. Convergence and comparison studies indicate that the proposed MIB method works very well for the vibration analysis of plates. In particular, modal bending moments and shear forces predicted by the proposed method vanish at boundaries for free edges. Copyright © 2008 John Wiley & Sons, Ltd.

Received 18 November 2007; Revised 26 February 2008; Accepted 26 February 2008

KEY WORDS: vibration of plates; matched interface and boundary method; free edge supports; high-order schemes

*Correspondence to: G. W. Wei, Department of Mathematics, Michigan State University, East Lansing, MI 48824, U.S.A.

†E-mail: wei@math.msu.edu

Contract/grant sponsor: NSF; contract/grant numbers: DMS-0616704, IIS-0430987

1. INTRODUCTION

Plates, beams, and shells are basic elements in engineering structures and are of great practical significance to civil, mechanical, and aerospace engineering. For instance, bridge slabs, floor systems, window glasses, and airplane wings can be modeled as plates or shells with various internal and boundary supports. A pioneer study in this field is due to Chladni [1], who analyzed the nodal patterns on square plates at their resonant frequencies. Apart from a few analytically solvable cases that are insignificant for real-world applications, there is no exact solution for most plates and structures encountered in engineering practices. As analytical methods often fail or become too cumbersome to use, numerical simulation is one of the major approaches in structural and mechanical engineering practice. Computational methods that determine the performance of numerical simulations have a crucial impact on the accuracy, robustness and reliability of structural analysis, and design.

In the past three decades, the vibration analysis of rectangular plates with uniform and non-uniform edge supports has attracted considerable attention. A variety of computational methods have been successfully employed for such analysis. Earlier success in the vibration analysis of plates includes methods of finite strip [2, 3], spline finite strip [4], Ritz variational methods [5, 6], Rayleigh methods [7], Galerkin approaches [8], and series expansions [9]. Recently, the least squares technique [10], meshless methods [11], Rayleigh–Ritz methods [12–17], and finite element methods [18, 19] have been introduced to the plate vibration analysis. Differential quadrature (DQ) methods [20–22] have found many successful applications in the vibration analysis. This method is based on the idea that the partial derivative of a function with respect to a spatial variable at a given discrete point can be expressed as a weighted linear sum of the function values at all the discrete points in the computational domain. Shu and Richards [23] introduced the generalized differential quadrature (GDQ) [24–26] to simplify the calculation of the weight coefficients. Their method has been successfully applied to the vibration analysis of plates with free edge supports [25, 26].

Nevertheless, a long-standing problem in the structural analysis is the prediction of modal bending moments and shear forces, which should vanish at boundaries for free edges. Except for methods designed with limited edge supports, such as the Levy-type solutions [27], no general numerical method has been reported to handle modal bending moments and shear forces for free edges, to our knowledge. This calls for new approaches in structural analysis.

All the above-mentioned methods are either local or global, with distinct advantages and disadvantages. Global methods are very accurate but are not flexible for irregular geometry and complex boundary conditions. In contrast, local methods are suitable for irregular geometry and complex boundary conditions but are less accurate than global ones. More recently, the discrete singular convolution (DSC) algorithm [28, 29] has emerged as a local spectral method to combine the accuracy of global methods with the flexibility of local methods. The mathematical foundation of the DSC algorithm is the theory of distributions and the theory of wavelets. The DSC algorithm has been realized in both collocation and Galerkin formulations [29–31]. The utility of the DSC algorithm for the vibration analysis has been extensively explored [29, 32–35], particularly for high-frequency problems [31, 36, 37]. The performance of the DSC algorithm for the vibration analysis has been independently studied by Civalek [38–40]. By extending the computational domain according to the boundary conditions, the DSC algorithm works well for simply supported, clamped, and transversely supported edges. Nonetheless, the earlier DSC algorithm has its difficulty in implementing the free edge conditions [29].

Most recently, the matched interface and boundary (MIB) method has been developed for solving partial differential equations with discontinuous coefficients and singular sources [41–44]. The MIB method is capable of dealing with arbitrarily complex interfaces and geometric singularities in three dimensions [45, 46]. The essential idea of the MIB method is to smoothly extend computational domains near the interface or the boundary so that the standard central finite difference (FD) discretization can be conveniently carried out. The interface or boundary conditions are strictly enforced in the domain extension. Although domain extensions were also commonly used in the DSC algorithm [29], each boundary condition is used only once. In contrast, the MIB method found a way to repeatedly use the lowest-order interface or boundary conditions, and thus is able to rigorously enforce complex conditions over a wider extended domain and achieve desirable higher-order accuracy [41]. This approach works because more regular grid function values are used in the enforcement of the interface or the boundary conditions. An interpolation formulation of the MIB method, in which one does not need to repeatedly enforce the interface or the boundary conditions, has also been proposed [43]. It becomes clear in this new formulation that the number of unknowns is consistent with the sum of the number of the interface (or the boundary) conditions and the number of function values on regular grid points. In a preliminary study, the MIB method has been utilized to overcome the difficulty of implementing free boundary conditions of beams in the DSC algorithm [47].

The objective of the present work is to introduce the MIB method for the vibration analysis of plates with arbitrary boundary supports and their arbitrary combinations. As the governing equation of plate vibration involves fourth-order derivatives, a normal stencil that would support a fourth-order discretization for an elliptic equation can only provide second-order accuracy in dealing with fourth-order equations. Therefore, wider extended domains are required to maintain high-order accuracy. The most challenging issue in the plate vibration analysis is the presence of cross derivatives in the boundary conditions of free edges and free corners. The present work overcomes these difficulties by developing a set of new MIB schemes, i.e. the domain extension cannot be pursued along a given meshline at a time as in the previous MIB schemes. The modal bending moments and shear forces predicted with the resulting MIB method vanish at free edges.

The remainder of this paper is organized as follows. In Section 2, we briefly review the governing equations of the plate vibration and three types of boundary conditions. In Section 3, theory and algorithm of the new MIB method is developed for plate vibration analysis. In Section 4, we validate the proposed MIB method by convergence studies. We select a few typical combinations of simply supported, clamped, and free edges to illustrate and validate the proposed method. Comparison is carried out against other established methods. Conclusion remarks are given in Section 5.

2. GOVERNING EQUATIONS

To establish notation and simplify our discussion, we briefly review the Kirchhoff theory of plates. The non-dimensional governing equation for the free vibration of a thin rectangular plate is given as [5]

$$\frac{\partial^4 u}{\partial X^4} + 2\lambda^2 \frac{\partial^4 u}{\partial X^2 \partial Y^2} + \lambda^4 \frac{\partial^4 u}{\partial Y^4} = \Omega^2 u \quad (1)$$

where u is the dimensionless transverse displacement and $X = x/l_x$ and $Y = y/l_y$ are dimensionless coordinates with l_x and l_y being the lengths of the plate edges. Here, $\lambda = l_x/l_y$ is the aspect ratio, $\Omega = \omega l_x^2 \sqrt{\rho h/D}$ is the dimensionless frequency with ω being the dimensional circular frequency, and $D = Eh^3[12(1-\nu^2)]$ being the flexural rigidity. Here, E is the Young modulus, ν is the Poisson ratio, ρ is the mass density of the plate material, and h is the plate thickness. Let us consider three typical types of boundary conditions for a rectangular plate, namely, simply supported, clamped, and free edges.

1. Simply supported edge (S)

$$u=0, \quad \frac{\partial^2 u}{\partial X^2}=0 \quad (2)$$

at $X = \text{constant}$ and

$$u=0, \quad \frac{\partial^2 u}{\partial Y^2}=0 \quad (3)$$

at $Y = \text{constant}$.

2. Clamped edge (C)

$$u=0, \quad \frac{\partial u}{\partial X}=0 \quad (4)$$

at $X = \text{constant}$ and

$$u=0, \quad \frac{\partial u}{\partial Y}=0 \quad (5)$$

at $Y = \text{constant}$.

3. Free edge (F)

$$\frac{\partial^2 u}{\partial X^2} + \nu \lambda^2 \frac{\partial^2 u}{\partial Y^2} = 0, \quad \frac{\partial^3 u}{\partial X^3} + (2-\nu) \lambda^2 \frac{\partial^3 u}{\partial X \partial Y^2} = 0 \quad (6)$$

at $X = \text{constant}$ and

$$\lambda^2 \frac{\partial^2 u}{\partial Y^2} + \nu \frac{\partial^2 u}{\partial X^2} = 0, \quad \lambda^2 \frac{\partial^3 u}{\partial Y^3} + (2-\nu) \frac{\partial^3 u}{\partial X^2 \partial Y} = 0 \quad (7)$$

at $Y = \text{constant}$ and

$$\frac{\partial^2 u}{\partial X \partial Y} = 0 \quad (8)$$

at the corner of two adjacent free edges. In most numerical approaches, it is the free edge boundary condition that requires special treatments. Certainly, the method developed in this work is able to handle other boundary conditions.

3. THEORY AND ALGORITHM

New MIB schemes are developed in this section for the eigenvalue problem of plate vibration analysis. We first present a second-order scheme that illustrates the algorithm of the MIB method. In the process of enforcing the given boundary conditions, all the fictitious values on the extended domain are resolved in terms of function values on the interior grid points. Therefore, the final discretization matrix for the governing equation is expressed solely on the information of interior grid points. After the illustration, we discuss the general MIB schemes for achieving arbitrarily high-order accuracy in the plate vibration analysis.

3.1. Second-order MIB scheme for plate vibration analysis

3.1.1. Domain extension. Let N_x and N_y be the total numbers of grid points in the x - and y -directions, respectively. To maintain a second-order discretization, we need to extend the computational domain by two layers of fictitious grid points at each edge, see Figure 1. One of these two layers of extended grid points is on the boundary. There are a total of $4(N_x - 2) + 4(N_y - 2) + 4$ grid points on the extended domains near four edges. For each grid point on the boundary, there are two boundary conditions. There is one boundary condition for each corner point. Therefore, the number of available boundary conditions is the same as the number of fictitious grid points ($4N_x + 4N_y - 12$).

The discretized boundary conditions for a grid point (i, j) on an edge can be expressed as

1. Simply supported edge

$$u_{i,j} = 0 \tag{9}$$

$$\sum_{k=0}^{N_x+1} c_{x,i,k}^{(2)} u_{k,j} = 0, \quad i = 1, N_x, \quad j = 2, \dots, N_y - 1 \tag{10}$$

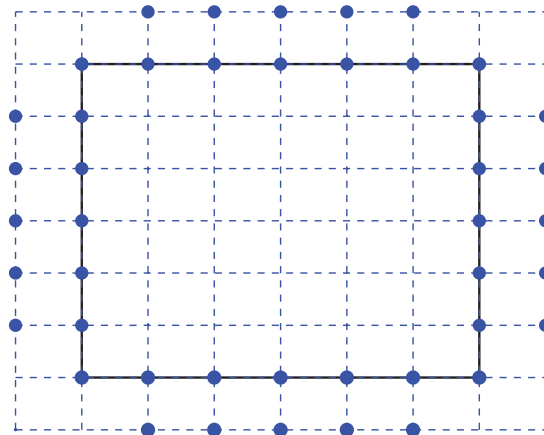


Figure 1. The distribution of first two layers of fictitious grid points ($N_x = N_y = 7, M = 2$). The solid line ‘—’ indicates the boundary of the plate.

at $X = \text{constant}$ and

$$u_{i,j} = 0 \quad (11)$$

$$\sum_{k=0}^{N_y+1} c_{y,j,k}^{(2)} u_{i,k} = 0, \quad i = 2, \dots, N_x - 1, \quad j = 1, N_y \quad (12)$$

at $Y = \text{constant}$. Here, c are FD coefficients and can be evaluated as described by Fornberg [48].

2. Clamped edge

$$u_{i,j} = 0 \quad (13)$$

$$\sum_{k=0}^{N_x+1} c_{x,i,k}^{(1)} u_{k,j} = 0, \quad i = 1, N_x, \quad j = 2, \dots, N_y - 1 \quad (14)$$

at $X = \text{constant}$ and

$$u_{i,j} = 0 \quad (15)$$

$$\sum_{k=0}^{N_y+1} c_{y,j,k}^{(1)} u_{i,k} = 0, \quad i = 2, \dots, N_x - 1, \quad j = 1, N_y \quad (16)$$

at $Y = \text{constant}$.

3. Free edge

$$\sum_{k=0}^{N_x+1} c_{x,i,k}^{(2)} u_{k,j} + v \lambda^2 \sum_{k=1}^{N_y} a_{y,j,k}^{(2)} u_{i,k} = 0 \quad (17)$$

$$\sum_{k=0}^{N_x+1} c_{x,i,k}^{(3)} u_{k,j} + (2-v) \lambda^2 \sum_{k=0}^{N_x+1} c_{x,i,k}^{(1)} \sum_{l=0}^{N_y+1} b_{y,j,k,l}^{(2)} u_{k,l} = 0$$

$$i = 1, N_x, \quad j = 2, \dots, N_y - 1 \quad (18)$$

at $X = \text{constant}$ and

$$\lambda^2 \sum_{k=0}^{N_y+1} c_{y,j,k}^{(2)} u_{i,k} + v \sum_{k=1}^{N_x} a_{x,i,k}^{(2)} u_{k,j} = 0 \quad (19)$$

$$\lambda^2 \sum_{k=0}^{N_y+1} c_{y,j,k}^{(3)} u_{i,k} + (2-v) \sum_{k=0}^{N_y+1} c_{y,j,k}^{(1)} \sum_{l=0}^{N_x+1} b_{x,i,k,l}^{(2)} u_{l,k} = 0$$

$$i = 2, \dots, N_x - 1, \quad j = 1, N_y \quad (20)$$

at $Y = \text{constant}$.

Here, i and j are the x - and y -indexes of the grid point where the boundary conditions are discretized, respectively. k and l are the summation indexes of differentiation. Here, $a_{x,i,k}^{(2)}$

$(i, k = 1, 2, \dots, N_x)$ are the FD coefficients [48] for $\partial^2 u / \partial X^2$ at $(X = i, Y = 1)$ and $(X = i, Y = N_y)$, respectively. Let vector $w_{x,i}^{(m)}(k_1 : k_2)$ denotes the FD coefficients on the k_1 th through the k_2 th grid points for the m th-order derivative at the i th point in the x -direction. And let vector $w_{y,j}^{(m)}(l_1 : l_2)$ denotes the FD coefficients on the l_1 th through the l_2 th grid points for the m th-order derivative at the j th point in the y -direction. Then the matrix representation of $a_{x,i,k}^{(2)}$ can be given as

$$(a_{x,i,k}^{(2)}) = \begin{bmatrix} a_{x,2,1}^{(2)} & \cdots & a_{x,2,N_x}^{(2)} \\ \vdots & \ddots & \vdots \\ a_{x,N_x-1,1}^{(2)} & \cdots & a_{x,N_x-1,N_x}^{(2)} \end{bmatrix} = \begin{bmatrix} w_{x,2}^{(2)}(1 : N_x) \\ \vdots \\ w_{x,N_x-1}^{(2)}(1 : N_x) \end{bmatrix}_{(N_x-2) \times N_x} \quad (21)$$

Here, $b_{x,i,k,l}^{(2)}$ are the FD coefficients for $\partial^2 u / \partial X^2$ at grid point (i, k) . Their matrix representation can be expressed as

$$(b_{x,i,k,l}) = \begin{bmatrix} 0 & 0 & b_{x,i,0,2}^{(2)} & \cdots \\ 0 & b_{x,i,1,1}^{(2)} & b_{x,i,1,2}^{(2)} & \cdots \\ b_{x,i,2,0}^{(2)} & b_{x,i,2,1}^{(2)} & b_{x,i,2,2}^{(2)} & \cdots \\ \vdots & \vdots & \vdots & \ddots \\ b_{x,i,N_x-1,0}^{(2)} & b_{x,i,N_x-1,1}^{(2)} & b_{x,i,N_x-1,2}^{(2)} & \cdots \\ 0 & b_{x,i,N_x,1}^{(2)} & b_{x,i,N_x,2}^{(2)} & \cdots \\ 0 & 0 & b_{x,i,N_x+1,2}^{(2)} & \cdots \\ \cdots & b_{x,i,0,N_x-1}^{(2)} & 0 & 0 \\ \cdots & b_{x,i,1,N_x-1}^{(2)} & b_{x,i,1,N_x}^{(2)} & 0 \\ \cdots & b_{x,i,2,N_x-1}^{(2)} & b_{x,i,2,N_x}^{(2)} & b_{x,i,2,N_x+1}^{(2)} \\ \ddots & \vdots & \vdots & \vdots \\ \cdots & b_{x,i,N_x-1,N_x-1}^{(2)} & b_{x,i,N_x-1,N_x}^{(2)} & b_{x,i,N_x-1,N_x+1}^{(2)} \\ \cdots & b_{x,i,N_x,N_x-1}^{(2)} & b_{x,i,N_x,N_x}^{(2)} & 0 \\ \cdots & b_{x,i,N_x+1,N_x-1}^{(2)} & 0 & 0 \end{bmatrix}$$

$$= \begin{bmatrix} 0 & 0 & w_{x,i}^{(2)}(2:N_x-1) & 0 & 0 \\ 0 & & w_{x,i}^{(2)}(1:N_x) & & 0 \\ & & w_{x,i}^{(2)}(0:N_x+1) & & \\ & & \vdots & & \\ & & w_{x,i}^{(2)}(0:N_x+1) & & \\ 0 & & w_{x,i}^{(2)}(1:N_x) & & 0 \\ 0 & 0 & w_{x,i}^{(2)}(2:N_x-1) & 0 & 0 \end{bmatrix}_{(N_y+2) \times (N_x+2)} \quad (22)$$

$c_{x,1,k}^{(m)}$ and $c_{x,N_x,k}^{(m)}$ ($m=1, 2, 3, k=0, 1, \dots, N_x+1$) are the FD coefficients for $\partial^m u / \partial X^m$ at $(1, j)$ and (N_x, j) , respectively. Their matrix representation can be expressed as

$$(c_{x,1,k}^{(m)}) = [c_{x,1,0}^{(m)} \quad c_{x,1,1}^{(m)} \quad \cdots \quad c_{x,1,N_x+1}^{(m)}] = [w_{x,1}^{(m)}(0:N_x+1)]_{1 \times (N_x+2)} \quad (23)$$

$$\begin{aligned} (c_{x,N_x,k}^{(m)}) &= [c_{x,N_x,0}^{(m)} \quad c_{x,N_x,1}^{(m)} \quad \cdots \quad c_{x,N_x,N_x+1}^{(m)}] \\ &= [w_{x,N_x}^{(m)}(0:N_x+1)]_{1 \times (N_x+2)} \end{aligned} \quad (24)$$

Similarly, $(a_{y,j,k}^{(2)})$, $(b_{y,j,k,l}^{(2)})$, and $(c_{y,j,k}^{(m)})$ are the FD coefficients for the partial derivatives with respect to Y . Their matrix representations can easily be obtained by changing subscription x into y in Equations (21)–(24).

At the corner of two free edges, the discretized boundary conditions can be expressed as

$$\sum_{k=1}^{N_x} e_{x,i,k}^{(1)} \sum_{l=0}^{N_y+1} q_{y,j,k,l}^{(1)} u_{k,l} = 0, \quad i=1, N_x, \quad j=1, N_y \quad (25)$$

where the matrix representations of $e_{x,i,k}^{(1)}$ and $q_{y,j,k,l}^{(1)}$ are

$$(e_{x,i,k}^{(1)}) = [w_{x,i}^{(1)}(1:N_x)]_{1 \times N_x} \quad (26)$$

$$(q_{y,j,k,l}^{(1)}) = \begin{bmatrix} 0 & w_{y,j}^{(1)}(1:N_x) & 0 \\ & w_{y,j}^{(1)}(0:N_x+1) & \\ & \vdots & \\ & w_{y,j}^{(1)}(0:N_x+1) & \\ 0 & w_{y,j}^{(1)}(1:N_x) & 0 \end{bmatrix}_{N_x \times (N_x+2)} \quad (27)$$

In order to provide a matrix representation of the fictitious values, we need to establish some notations. Referring to Figure 1, we denote the fictitious values by a vector F_M , where $M=2$ is a stencil parameter. The k -component of F_2 , $F_{2,k}$, is denoted by

$$F_{2,k} = u_{i,j} \quad (28)$$

where the index k is restricted to

$$k = \begin{cases} i-1 & \forall 2 \leq i \leq N_x - 1, \quad j=0 \\ N_x - 2 + i & \forall 1 \leq i \leq N_x, \quad j=1 \\ N_x - 2 + N_x + 4(j-2) + 1 + i & \forall 0 \leq i \leq 1, \quad 2 \leq j \leq N_y - 1 \\ N_x - 2 + N_x + 4(j-2) + 3 + i - N_x & \forall N_x \leq i \leq N_x + 1, \quad 2 \leq j \leq N_y - 1 \\ N_x - 2 + N_x + 4(N_y - 2) + i & \forall 1 \leq i \leq N_x, \quad j = N_y \\ N_x - 2 + N_x + 4(N_y - 2) + N_x + i - 1 & \forall 2 \leq i \leq N_x - 1, \quad j = N_y + 1 \end{cases} \quad (29)$$

Here, the label k counts only all the fictitious points.

To resolve the elements of F_2 , we consider a matrix representation of the form

$$F_2 = C_2 U \quad (30)$$

where vector U denote all the function values on the interior grid points. The components of U are given by $U_k = u_{i,j}$ with

$$k = (j-2)(N_x - 2) - 1 + i \quad \forall 2 \leq i \leq N_x - 1, \quad 2 \leq j \leq N_y - 1 \quad (31)$$

Here, the label k counts only all the interior points. The matrix C_2 can be determined as the follows. First, let us cast the discretized boundary conditions (9)–(20) and (25) in the matrix form

$$A_{bF_2} \cdot F_2 + A_{bU} \cdot U = 0 \quad (32)$$

where A_{bF_2} and A_{bU} , respectively, represent the coefficient matrix of fictitious values F_2 and interior grid point values. By using Equation (30), the above equation can be rewritten:

$$A_{bF_2} \cdot C_2 U + A_{bU} \cdot U = 0 \quad (33)$$

Therefore, we can determine matrix C :

$$C_2 = -A_{bF_2}^{-1} \cdot A_{bU} \quad (34)$$

It is noted that the dimensions of matrices A_{bF_2} and A_{bU} are $(4N_x + 4N_y - 12)$ by $(4N_x + 4N_y - 12)$ and $(4N_x + 4N_y - 12)$ by $(N_x - 2)(N_y - 2)$, respectively.

3.1.2. Discretization matrix. The above section provides a representation of fictitious values in terms of the function values on the interior grid points by using the boundary conditions. This

enables us to construct a matrix representation of the governing equation solely in terms of function values on the interior grid points. A second-order discretization ($M=2$) of the governing equation can be given

$$\sum_{k=-2}^2 s_{x,k}^{(4)} u_{i+k,j} + 2\lambda^2 \cdot \sum_{k=-2}^2 s_{x,k}^{(2)} \sum_{l=0}^{N_y+1} t_{y,i+k,j,l}^{(2)} u_{i+k,l} + \sum_{k=-2}^2 s_{y,k}^{(4)} u_{i,j+k} = \Omega^2 \cdot u_{i,j} \quad (35)$$

with $2 \leq i \leq N_x - 1$, $2 \leq j \leq N_y - 1$. Here, $s_{x,k}^{(m)}$ and $s_{y,k}^{(m)}$ are central FD coefficients, which can be expressed as

$$(s_{x,k}^{(m)}) = w_{x,0}^{(m)}(-2:2), \quad (s_{y,k}^{(m)}) = w_{y,0}^{(m)}(-2:2) \quad (36)$$

Here, $t_{y,i+k,j,l}^{(2)}$ are the FD coefficients for $\partial^2 u / \partial Y^2$ at $(i+k, j)$. When $2 \leq i+k \leq N_x - 1$, they are standard central FD coefficients. The matrix representation of $t_{y,i+k,j,l}^{(2)}$ can be expressed as

$$(t_{y,i+k,j,l}^{(2)}) = \begin{bmatrix} w_{y,2}^{(2)}(0:4) & 0 & 0 & 0 & 0 \\ 0 & w_{y,3}^{(2)}(1:5) & 0 & 0 & 0 \\ 0 & 0 & \ddots & 0 & 0 \\ 0 & 0 & 0 & w_{y,j}^{(2)}(j-2:j+2) & 0 \\ 0 & 0 & 0 & 0 & 0 \\ 0 & 0 & 0 & 0 & 0 \\ 0 & 0 & & & \\ 0 & 0 & & & \\ 0 & 0 & & & \\ \vdots & 0 & & & \\ 0 & w_{y,N_y-1}^{(2)}(N_y-3:N_y+1) \end{bmatrix}_{(N_y-2) \times (N_y+2)} \quad (37)$$

Note that $w_{y,2}^{(2)}(0:4) = w_{y,3}^{(2)}(1:5) = w_{y,j}^{(2)}(j-2:j+2) = w_{y,N_y-1}^{(2)}(N_y-3:N_y+1)$ as all of them are standard central FD schemes with the same bandwidth. Near the corners, i.e. when $i+k = 0, 1, N_x, N_x + 1$, the standard central FD schemes cannot be used in the cross derivatives because there are not enough grid points on the side where grid point $(i+k, j)$ is near the upper or lower side of the plate. Therefore, asymmetric (i.e. one-sided) FD schemes are used in these cases.

Parameter $L \geq 2$ is used to describe the bandwidth of the derivatives

$$\begin{aligned}
 & \mathbf{t}_{y,i+k,j,l}^{(2)} \\
 & \left[\begin{array}{ccccc}
 w_{y,2}^{(2)}(2:2+L) & 0 & 0 & 0 & 0 \\
 \vdots & \vdots & \vdots & \vdots & \vdots \\
 w_{y,2+L/2}^{(2)}(2:2+L) & 0 & 0 & 0 & 0 \\
 0 & w_{y,3+L/2}^{(2)}(3:3+L) & 0 & 0 & 0 \\
 0 & 0 & \ddots & 0 & 0 \\
 0 & 0 & 0 & w_{y,j}^{(2)}(j-L/2:j+L/2) & 0 \\
 0 & 0 & 0 & 0 & \ddots \\
 0 & 0 & 0 & 0 & 0 \\
 0 & 0 & 0 & 0 & 0 \\
 \vdots & \vdots & \vdots & \vdots & \vdots \\
 0 & 0 & 0 & 0 & 0 \\
 \\
 0 & & & 0 & \\
 \vdots & & & \vdots & \\
 0 & & & 0 & \\
 0 & & & 0 & \\
 0 & & & 0 & \\
 0 & & & 0 & \\
 0 & & & 0 & \\
 w_{y,N_y-2-L/2}^{(2)}(N_y-2-L:N_y-2) & & & 0 & \\
 0 & & & w_{y,N_y-1-L/2}^{(2)}(N_y-1-L:N_y-1) & \\
 \vdots & & & \vdots & \\
 0 & & & w_{y,N_y-1}^{(2)}(N_y-1-L:N_y-1) &
 \end{array} \right]_{(N_y-2) \times (N_y-2)}
 \end{aligned} \tag{38}$$

The FD weights in the first and the last $L/2$ rows are different from each other as one-sided FD schemes are used. The FD weights in the middle rows are the same as they are standard central

FD weights with the same bandwidth. Finally, the discretized governing equation can be expressed in the following matrix form:

$$A_{gF_2} \cdot F_2 + A_{gU} \cdot U = \Omega^2 \cdot U \tag{39}$$

where A_{gF_2} and A_{gU} represent the coefficient matrix of fictitious values and function values on interior points obtained from the discretized governing equation in Equation (35). Substituting Equation (34) into Equation (39), one obtains

$$(A_{gF_2} \cdot A_{bF_2}^{-1} \cdot A_{bU} + A_{gU}) \cdot U = \Omega^2 \cdot U \tag{40}$$

It is noted that the dimensions of matrices A_{gF_2} and A_{gU} are $(N_x - 2) \cdot (N_y - 2)$ by $(4N_x + 4N_y - 12)$ and $(N_x - 2) \cdot (N_y - 2)$ by $(N_x - 2) \cdot (N_y - 2)$, respectively. Finally, Equation (40) is to be solved for the eigenvector U and eigenvalues.

3.2. High-order MIB schemes

To construct high-order MIB schemes, we first create more fictitious values outside the boundary. For example, three layers of fictitious values are needed for a fourth-order MIB scheme. Let M denotes the total number of layers of fictitious points. In general, M layers of fictitious values can be used to construct $(2M - 2)$ th-order MIB scheme. Unfortunately, the total number of the boundary conditions is fixed. One therefore encounters a situation that the number of unknowns (i.e. fictitious values) is greater than the number of equations (i.e. boundary conditions). This difficulty has been resolved in the MIB method by repeatedly using the boundary conditions [41] and appropriate interior function values. This idea and its implementation details were discussed in the original work of the MIB method [41].

3.2.1. Domain extension. To obtain a matrix representation of the fictitious values, we provide an iterative scheme. Assume that the first $p - 1$ layers of fictitious points have been found as shown in Figure 2 and can be expressed as

$$F_{p-1} = C_{p-1} U \tag{41}$$

We look for the expression of F_p in terms of C_{p-1} and U .

There are $2N_x + 2N_y - 8$ fictitious points on each layer except the first one. To obtain the matrix representation of the p th layer of fictitious values, $2N_x + 2N_y - 8$ unknowns can be solved from $4N_x + 4N_y - 8$ boundary conditions on $2N_x + 2N_y - 4$ edge points. Therefore, only one boundary condition on each non-corner edge point, i.e. Equations (10), (12), (14), (16), (17), and (19), is required. In fact, each boundary condition has to be enforced at least once. After the first round enforcement of all boundary conditions, we normally use only the easy-to-implement boundary condition. In order to involve all the p layers of fictitious points in these boundary conditions, the FD coefficients $c_{x,1,k}^{(m)}$, $c_{x,N_x,k}^{(m)}$, $c_{y,1,k}^{(m)}$, and $c_{y,N_y,k}^{(m)}$ in these equations should have the following matrix representations:

$$\begin{aligned} (c_{x,1,k}^{(m)}) &= w_{x,1}^{(m)} (2 - p : L + 1), & (c_{x,N_x,k}^{(m)}) &= w_{x,N_x}^{(m)} (N_x - L : N_x + p - 1) \\ (c_{y,1,k}^{(m)}) &= w_{y,1}^{(m)} (2 - p : L + 1), & (c_{y,N_y,k}^{(m)}) &= w_{y,N_y}^{(m)} (N_y - L : N_y + p - 1) \end{aligned} \tag{42}$$

MATCHED INTERFACE AND BOUNDARY (MIB) METHOD

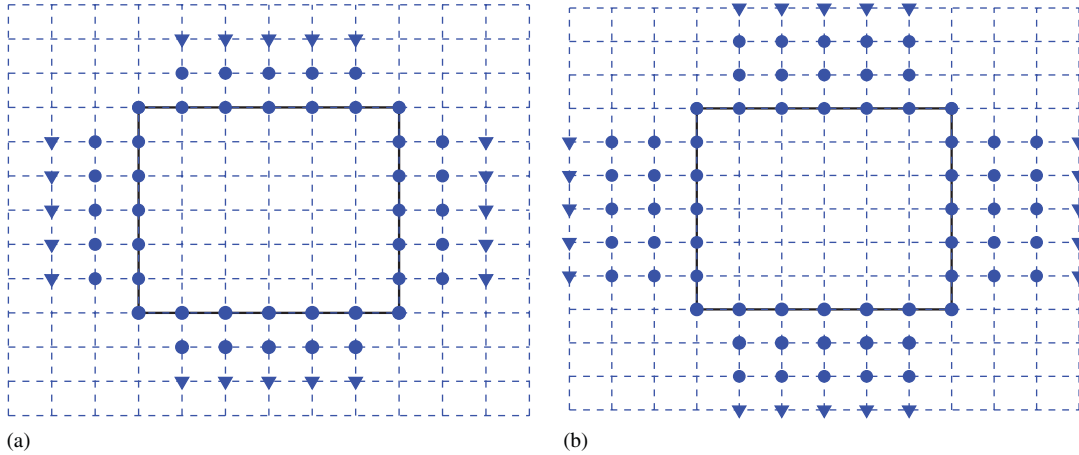


Figure 2. The distribution of fictitious points: (a) $p=3$ and (b) $p=4$; ‘▼’ indicates the next layer of fictitious points to be extended and ‘●’ indicates the fictitious points that have already been found by previous steps.

where L is the bandwidth of the FD coefficients. The FD coefficients $a_{x,i,k}^{(2)}$ for $\partial^2 u / \partial X^2$, at points $(i, 1)$ and (i, N_y) , and the FD coefficients $a_{y,j,k}^{(2)}$ for $\partial^2 u / \partial Y^2$, at points $(1, j)$ and (N_x, j) , are also defined with bandwidth $L+1$ to achieve better stability. These matrix representations are given as

$$(a_{x,i,k}^{(2)}) = \begin{bmatrix} w_{x,2}^{(2)}(1:L+1) & 0 & 0 & 0 \\ \vdots & \vdots & \vdots & \vdots \\ w_{x,1+L/2}^{(2)}(1:L+1) & 0 & 0 & 0 \\ 0 & w_{x,2+L/2}^{(2)}(2:L+2) & 0 & 0 \\ 0 & 0 & \ddots & 0 \\ 0 & 0 & 0 & w_{x,i}^{(2)}(i-L/2:i+L/2) \\ 0 & 0 & 0 & 0 \\ 0 & 0 & 0 & 0 \\ 0 & 0 & 0 & 0 \\ \vdots & \vdots & \vdots & \vdots \\ 0 & 0 & 0 & 0 \end{bmatrix}$$

$$\begin{array}{ccc}
 0 & 0 & 0 \\
 \vdots & \vdots & \vdots \\
 0 & 0 & 0 \\
 0 & 0 & 0 \\
 0 & 0 & 0 \\
 0 & 0 & 0 \\
 \ddots & 0 & 0 \\
 0 & w_{x,N_x-2-L/2}^{(2)}(N_x-1-L:N_x-1) & 0 \\
 0 & 0 & w_{x,N_x-L/2}^{(2)}(N_x-L:N_x) \\
 \vdots & \vdots & \vdots \\
 0 & 0 & w_{x,N_x-1}^{(2)}(N_x-L:N_x)
 \end{array} \Bigg]_{(N_x-2) \times (N_x)} \quad (43)$$

and

$$(a_{y,j,k}^{(2)}) = \begin{bmatrix}
 w_{y,2}^{(2)}(1:L+1) & 0 & 0 & 0 \\
 \vdots & \vdots & \vdots & \vdots \\
 w_{y,1+L/2}^{(2)}(1:L+1) & 0 & 0 & 0 \\
 0 & w_{y,2+L/2}^{(2)}(2:L+2) & 0 & 0 \\
 0 & 0 & \ddots & 0 \\
 0 & 0 & w_{y,j}^{(2)}(j-L/2:j+L/2) & 0 \\
 0 & 0 & 0 & 0 \\
 0 & 0 & 0 & 0 \\
 0 & 0 & 0 & 0 \\
 0 & 0 & 0 & 0 \\
 0 & 0 & 0 & 0
 \end{bmatrix}$$

$$\begin{array}{ccc}
 0 & 0 & 0 \\
 \vdots & \vdots & \vdots \\
 0 & 0 & 0 \\
 0 & 0 & 0 \\
 0 & 0 & 0 \\
 0 & 0 & 0 \\
 \ddots & 0 & 0 \\
 0 & w_{y,N_y-1-L/2}^{(2)}(N_y-1-L:N_y-1) & 0 \\
 0 & 0 & w_{y,N_y-L/2}^{(2)}(N_y-L:N_y) \\
 \vdots & \vdots & \vdots \\
 0 & 0 & w_{y,N_y-1}^{(2)}(N_y-L:N_y)
 \end{array} \Bigg]_{(N_y-2) \times (N_y)} \quad (44)$$

The matrix representation of $2N_x + 2N_y - 8$ boundary conditions can be expressed as

$$A_{eF_e} \cdot F_e + A_{eF_{p-1}} \cdot F_{p-1} + A_{eU} \cdot U = 0 \quad (45)$$

where vector F_e denotes the p th layer of fictitious values. The dimensions of matrices A_{eF_e} , $A_{eF_{p-1}}$, and A_{eU} are $(2N_x + 2N_y - 8) \times (2N_x + 2N_y - 8)$, $(2N_x + 2N_y - 8) \times (2(p-1)N_x + 2(p-1)N_y - 8(p-1) + 4)$, and $(2N_x + 2N_y - 8) \times (N_x - 2) \cdot (N_y - 2)$, respectively. Combining Equation (41) with Equation (45), one obtains

$$A_{eF_e} \cdot F_e + A_{eF_{p-1}} \cdot C_{p-1} \cdot U + A_{eU} \cdot U = 0 \quad (46)$$

Here, one can resolve F_e

$$F_e = -A_{eF_e}^{-1} \cdot (A_{eF_{p-1}} \cdot C_{p-1} + A_{eU}) \cdot U = C_e \cdot U \quad (47)$$

Therefore, the p layers of fictitious values can be represented in terms of interior points

$$F_p = C_p U \quad (48)$$

where $C_p = C_e \oplus C_{p-1}$.

By repeating the above procedure until $p = M$, we will have the matrix representation of M layers of fictitious values in terms of interior values

$$F_M = C_M U \quad (49)$$

where the vector of interior values having its components $U_k = u_{i,j}$ as defined earlier. Here, F_M 's k -component, $F_{M,k}$, is defined by

$$F_{M,k} = u_{i,j} \quad (50)$$

where the index k is restricted to

$$k = \begin{cases} (M-2+j)(N_x-2)+i-1 & \forall 2 \leq i \leq N_x-1, -M+2 \leq j \leq 0 \\ (M-1)(N_x-2)+i & \forall 1 \leq i \leq N_x, j=1 \\ (M-1)(N_x-2)+N_x+2M(j-2)+M-1+i \\ \quad \forall -M+2 \leq i \leq 1, 2 \leq j \leq N_y-1 \\ (M-1)(N_x-2)+N_x+2M(j-2)+M+1+i-N_x \\ \quad \forall -M+2 \leq i \leq 1, 2 \leq j \leq N_y-1 \\ (M-1)(N_x-2)+N_x+2M(N_y-2)+i & \forall 1 \leq i \leq N_x, j=N_y \\ (M-1)(N_x-2)+N_x+2M(N_y-2)+N_x+(j-(N_y+1))(N_x-2)+i-1 \\ \quad \forall 2 \leq i \leq N_x-1, N_y+1 \leq j \leq N_y+M+1 \end{cases} \quad (51)$$

Here, we count only all the fictitious points.

3.3. Discretization matrix

The governing equation can now be discretized by $2(M-1)$ th-order MIB schemes as

$$\sum_{k=-M}^M s_{x,k}^{(4)} u_{i+k,j} + 2\lambda^2 \cdot \sum_{k=-M}^M s_{x,k}^{(2)} \sum_{l=0}^{N_y+1} t_{y,i+k,j,l}^{(2)} u_{i+k,l} + \sum_{k=-M}^M s_{y,k}^{(4)} u_{i,j+k} = \Omega^2 \cdot u_{i,j} \quad (52)$$

with $2 \leq i \leq N_x-1, 2 \leq j \leq N_y-1$. $s_{x,k}^{(m)}$ and $s_{y,k}^{(m)}$ are M th-order central FD coefficients, which can be expressed as

$$(s_{x,k}^{(m)}) = w_{x,0}^{(m)}(-M:M), \quad (s_{y,k}^{(m)}) = w_{y,0}^{(m)}(-M:M) \quad (53)$$

The matrix representation of $t_{y,i+k,j,l}^{(2)}$ can be expressed as

$$(t_{y,i+k,j,l}^{(2)}) = \begin{bmatrix} w_{y,2}^{(2)}(2-M:2+M) & 0 & 0 & 0 \\ 0 & w_{y,3}^{(2)}(3-M:3+M) & 0 & 0 \\ 0 & 0 & \ddots & 0 \\ 0 & 0 & 0 & w_{y,j}^{(2)}(j-M:j+M) \\ 0 & 0 & 0 & 0 \\ 0 & 0 & 0 & 0 \end{bmatrix}$$

$$\begin{array}{cc}
 0 & 0 \\
 0 & 0 \\
 0 & 0 \\
 0 & 0 \\
 \vdots & 0 \\
 0 & w_{y,N_y-1}^{(2)}(N_y-1-M:N_y-1+M)
 \end{array} \Bigg]_{(N_y-2) \times (N_y-2+2M)} \quad (54)$$

when $2 \leq i+k \leq N_x-1$. Similar to Equation (37) in the second-order scheme, all the non-zero weights in each row are the same. $(t_{y,i+k,j,l}^{(2)})$ is given by Equation (38) when $2-2M \leq i+k \leq 1$ or $N_x \leq i+k \leq N_x+2M-1$.

The governing equation can be expressed in the following matrix form:

$$A'_{gF_M} \cdot F_M + A'_{gU} \cdot U = \Omega^2 \cdot U \quad (55)$$

Substituting Equation (41) into Equation (55), one obtains

$$(A'_{gF_M} \cdot C_M + A'_{gU}) \cdot U = \Omega^2 \cdot U \quad (56)$$

The dimensions of matrices A'_{gF_M} and A'_{gU} are $(N_x-2) \cdot (N_y-2) \times (2MN_x+2MN_y-8M+4)$ and $(N_x-2) \cdot (N_y-2) \times (N_x-2) \cdot (N_y-2)$, respectively.

4. RESULTS AND DISCUSSION

In this section, we demonstrate the utility, test convergence and examine the accuracy of proposed new MIB method for the vibration analysis of square plates. We consider three boundary conditions, the simply supported (S), clamped (C), and free (F) edges. An FSCS plate will have a free edge along $X=0$, a simply supported edge along $Y=0$, a clamped edge along $X=1$, and a simply supported edge along $Y=1$, respectively. The performance of the proposed method is also explored on a few typical combinations of these three edges. Special attention is paid to free edges and their combinations with other two types of edges. As the convergence can be improved by using adaptive grids, we also constructed the present MIB method in non-uniform Chebyshev grids. Comparison is made to the results of the GDQ method [25]. As an established global method, the GDQ method is known for its accuracy in the vibration analysis of rectangular plates. A standard eigen solver is used to obtain eigenvectors and eigenvalues. To evaluate the performance, we compute the relative L_2 'error' by using the first five eigenvalues

$$L_2 = \sqrt{\frac{1}{5} \sum_{i=1}^5 \left(\frac{|\Omega_i - \Omega_i^e|}{\Omega_i^e} \right)^2} \quad (57)$$

where Ω^e are the reference frequency data of Leissa [5] or Leissa and Narita [6]. As there is no exact solution to many plates studied, most 'errors' mentioned in this paper should be understood as the differences with respect to the reference.

4.1. Uniform meshes

Let us consider the computational domain of $[0, 1] \times [0, 1]$. The coordinates of uniform grid points are chosen as

$$X_i = \frac{i-1}{N_x-1}, \quad 2L-2 \leq i \leq N_x+2L-1 \quad (58)$$

$$Y_j = \frac{j-1}{N_y-1}, \quad 2L-2 \leq j \leq N_y+2L-1 \quad (59)$$

The convergence analysis of plates with different edge supports is presented in Tables I–X. In these tables, $N = N_x = N_y$ is the number of grid points used for the discretization in each dimension. Thus, $N=7$ represents a 7×7 mesh. The half bandwidth of the discretization is given by M , which also represents the number of layers of fictitious values extended along each boundary.

Table I. Convergence of the SSSS plate.

M	L	N	Ω_1	Ω_2	Ω_3	Ω_4	Ω_5	L_2
2	6	7	19.510	46.029	46.100	74.362	80.222	9.74E-2
		9	19.611	47.739	47.743	76.882	90.335	4.48E-2
		11	19.657	48.297	48.297	77.617	92.856	3.07E-2
		13	19.683	48.618	48.618	78.036	94.649	2.13E-2
3	8	9	10.735	49.063	49.135	78.720	95.198	1.63E-2
		11	19.738	49.281	49.288	78.863	97.963	3.46E-3
		13	19.739	49.313	49.314	78.910	98.162	2.47E-3
		15	19.739	49.330	49.330	78.933	98.455	1.13E-3
4	11	11	19.739	49.341	49.346	78.943	98.799	4.79E-4
		13	19.739	49.346	49.346	78.955	98.620	3.43E-4
		15	19.739	49.347	49.347	78.956	98.679	7.67E-5
		17	19.739	49.348	49.348	78.956	98.688	3.44E-5
Reference [5]			19.739	49.348	49.348	78.957	98.696	

Table II. Convergence of the CCCC plate.

M	L	N	Ω_1	Ω_2	Ω_3	Ω_4	Ω_5	L_2
2	6	7	36.229	68.497	68.518	103.539	103.659	1.06E-1
		9	36.151	71.448	71.451	107.281	120.213	4.26E-2
		11	36.100	72.141	72.142	107.780	123.492	2.99E-2
		13	36.068	72.544	72.544	107.993	126.085	2.04E-2
3	8	9	35.885	72.339	72.387	106.946	124.969	2.50E-2
		11	35.935	73.033	73.038	107.618	129.674	7.94E-3
		13	35.946	73.167	73.167	107.718	130.297	5.55E-3
		15	35.964	73.266	73.266	107.904	130.939	3.11E-3
4	11	11	35.990	73.385	73.386	108.259	131.436	7.34E-4
		13	35.988	73.401	73.401	108.263	131.484	5.41E-4
		15	35.986	73.396	73.396	108.242	131.560	3.37E-4
		17	35.985	73.394	73.394	108.225	131.573	3.46E-4
Reference [5]			35.992	73.413	73.413	108.270	131.640	

Table III. Convergence of the FSSS plate.

M	L	N	Ω_1	Ω_2	Ω_3	Ω_4	Ω_5	L_2
2	6	7	11.714	27.672	34.557	55.264	56.663	8.63E-2
		9	11.676	27.704	40.479	59.123	59.643	1.79E-2
		11	11.682	27.729	40.326	58.739	60.403	1.43E-2
		13	11.684	27.740	40.606	58.857	60.858	9.81E-3
3	8	9	11.632	14.177	14.177	27.739	42.686	4.58E-1
		11	11.682	27.743	37.346	57.609	61.639	4.33E-2
		13	11.681	27.748	48.345	55.034	55.034	9.69E-2
		15	11.683	27.752	41.265	59.098	61.808	8.70E-4
4	11	11	11.682	27.743	37.346	57.609	61.639	4.33E-2
		13	11.685	27.756	41.352	59.183	61.859	1.90E-3
		15	11.685	27.756	41.193	59.064	61.859	5.50E-5
		17	11.684	27.757	41.196	59.066	61.860	3.13E-5
GDQ		15	11.685	27.756	41.197	59.066	61.861	0.00E-0
Reference [5]			11.685	27.756	41.197	59.066	61.861	

Table IV. Convergence of the FCCC plate.

M	L	N	Ω_1	Ω_2	Ω_3	Ω_4	Ω_5	L_2
2	6	7	24.257	41.402	56.145	71.334	77.538	6.51E-2
		9	24.238	40.949	60.878	75.203	80.984	2.33E-2
		11	24.202	40.709	61.807	75.819	80.940	1.55E-2
		13	24.157	40.547	62.517	76.161	81.095	1.01E-2
3	8	9	24.231	40.198	63.146	63.146	66.383	1.12E-1
		11	24.682	40.538	58.197	76.489	78.650	4.13E-2
		13	23.738	39.051	62.029	71.671	71.671	6.04E-2
		15	24.381	40.014	63.630	76.489	80.351	7.26E-3
4	10	11	24.118	40.353	61.677	76.850	80.019	1.39E-2
		13	23.665	40.073	63.766	76.933	81.259	7.59E-3
		15	23.987	40.194	63.325	76.913	80.809	2.42E-3
		17	23.985	40.194	63.454	76.913	80.967	2.50E-3
GDQ		15	24.025	40.147	63.494	76.845	80.901	1.67E-3
Reference [5]			24.020	40.039	63.493	76.761	80.713	

As M increases, the convergence order of the MIB schemes increases. We use L to represent the stencil width used for calculating fictitious values. In the present work, N , M , and L together determine the accuracy of the numerical results. Once L is given, M could be increased to certain level to obtain stable and highly accurate results. However, the accuracy is eventually constrained by L . Therefore, in Tables I–V, the value of M is associated with the value of L . That is, $M=2$ when $L=6$, $M=3$ when $L=8$, and $M=4$ when $L=11$. Choosing an M that is relatively larger than a fixed L will not increase the order of accuracy, but it may make the numerical solutions more stable, which is a crucial feature for plates with at least one free corner.

Table I gives the convergence analysis for the SSSS plate, which admits an analytical solution. This is a relatively easy case. The proposed MIB method shows an excellent convergence trend as M and N increase.

Table V. Convergence of the FFSS plate.

M	L	N	Ω_1	Ω_2	Ω_3	Ω_4	Ω_5	L_2
2	6	7	2.729	15.248	17.792	37.094	48.009	1.12E-1
		9	3.089	17.391	18.878	38.220	44.457	7.13E-2
		11	3.238	17.363	19.042	38.320	49.842	2.29E-2
		13	3.320	17.350	19.151	38.401	50.357	1.19E-2
3	8	9	14.691	17.633	20.100	34.884	34.884	1.51E-0
		11	4.013	17.292	22.196	41.877	41.877	1.42E-1
		13	3.563	17.306	20.067	39.674	40.018	1.04E-1
4	11	15	3.339	17.311	19.300	38.287	51.012	5.66E-3
		11	4.069	17.317	22.266	43.893	43.893	1.47E-1
		13	3.784	17.320	20.500	39.629	51.145	6.30E-2
		15	3.483	17.321	19.623	38.647	51.089	1.70E-2
GDQ		17	3.394	17.320	19.277	38.257	51.078	4.97E-3
		15	2.549	17.316	17.662	36.576	51.039	1.18E-1
Reference [5]			3.369	17.407	19.367	38.291	51.324	

Table VI. Convergence of the FFSC plate.

M	L	N	Ω_1	Ω_2	Ω_3	Ω_4	Ω_5	L_2
2	6	7	4.772	20.235	20.235	41.746	51.279	1.00E-1
		9	4.921	19.344	24.460	42.767	49.634	4.73E-2
		11	4.781	19.296	24.801	43.297	52.463	4.89E-2
		13	4.908	19.455	24.677	43.135	52.747	3.87E-2
3	7	9	3.129	17.183	19.274	25.322	43.949	2.95E-1
		11	4.044	20.18	24.31	43.46	52.593	1.13E-1
		13	7.710	21.567	21.567	43.271	51.026	2.12E-1
4	7	15	5.778	19.528	24.428	43.475	53.828	3.68E-2
		11	4.686	20.535	24.506	43.898	54.736	6.70E-2
		13	8.252	21.295	21.295	43.179	52.351	2.54E-1
		15	5.746	19.467	24.553	43.597	53.701	3.36E-2
GDQ		17	5.419	19.210	24.853	43.559	53.214	6.50E-3
		15	5.780	20.703	20.926	40.296	52.255	9.07E-2
Reference [5]			5.364	19.171	24.768	43.191	53.000	

The results for the CCCC plate are given in Table II. The numerical results are very close to the solutions of Leissa [5]. As the computational grid size N and the order of the MIB scheme M increase, the numerical solutions converge to the ones in Reference [5] very fast. Under the same N , the larger M and L usually result in smaller errors.

We next consider plates with one free edge. Tables III and IV show the convergence analysis of FSSS and FCCC plates, respectively. The numerical results of the GDQ method [25] with the mesh size of 15×15 are provided for a comparison. Both cases involve a free edge that is designed to test the proposed algorithm. The convergence of the numerical solutions to the ones in Reference [5] is very fast. When the mesh size is 15×15 , the relative error L_2 for the FSSS plate is 8.7×10^{-4} for $M=3$ and 5.5×10^{-5} for $M=4$. With the same mesh size, the relative error L_2 for the FCCC plate is 7.3×10^{-3} for $M=3$ and 2.4×10^{-3} for $M=4$. These differences again indicate that it is relatively easy to deal with simply supported edges. The numerical results also

MATCHED INTERFACE AND BOUNDARY (MIB) METHOD

Table VII. Convergence of the FFCC plate.

M	L	N	Ω_1	Ω_2	Ω_3	Ω_4	Ω_5	L_2
2	6	7	6.465	22.119	25.469	48.406	60.285	5.52E-2
		9	6.386	24.668	25.090	40.059	40.059	1.84E-1
		11	6.919	24.244	27.969	44.640	61.676	3.80E-2
		13	7.068	24.210	27.737	46.397	61.981	2.48E-2
3	6	9	3.727	20.375	24.557	24.557	47.760	3.28E-1
		11	8.696	23.148	25.602	47.405	61.942	1.16E-1
		13	18.003	18.003	24.454	44.430	44.430	7.35E-1
4	9	15	8.154	24.125	26.764	50.101	63.415	8.11E-2
		11	5.252	24.199	33.573	45.287	45.287	2.04E-1
		13	3.716	23.677	29.657	54.279	63.305	2.22E-1
		15	7.149	24.323	26.249	47.865	62.719	1.63E-2
GDQ Reference [5]		17	6.542	23.735	25.747	47.547	62.692	3.08E-2
		15	7.873	23.615	23.873	44.587	62.730	8.23E-2
			6.942	24.034	26.681	47.785	63.039	

Table VIII. Convergence of the FFSS plate.

M	L	N	Ω_1	Ω_2	Ω_3	Ω_4	Ω_5	L_2
2	6	7	5.660	12.013	19.158	26.226	47.165	1.58E-1
		9	6.068	14.981	25.270	25.699	39.212	9.59E-2
		11	6.306	14.827	25.005	26.048	46.947	3.00E-2
		13	6.618	14.801	25.337	26.655	47.648	1.52E-2
3	8	9	11.815	11.815	20.797	25.391	25.684	4.26E-1
		11	8.474	15.118	30.600	37.322	37.322	2.66E-1
		13	7.318	14.954	26.850	28.249	49.635	6.32E-2
		15	6.605	14.894	25.393	26.119	48.601	5.19E-3
4	8	11	8.684	15.113	29.525	38.934	38.934	2.83E-1
		13	6.900	14.979	25.673	27.157	48.596	2.60E-2
		15	6.866	14.919	25.934	26.347	48.598	1.73E-2
		17	6.666	14.912	25.436	26.171	48.475	4.32E-3
GDQ Reference [5]		15	5.161	14.725	23.082	24.156	46.296	1.16E-1
			6.648	15.023	25.492	26.126	48.711	

show that when N is relatively small, i.e. $N < 13$, $M = 2$ is a better choice than $M = 3$ and 4. The GDQ method [25] produces similar but slight better accuracy in these two cases. Nevertheless, the proposed MIB method works well for plates involving one free edge.

We next consider a few plates with one free corner, which is a more challenging situation. Tables V, VII, and VII show the convergence analysis of FFSS, FFSC, and FFCC plates, respectively. For the GDQ method [25], when a uniform grid is applied, the relative error L_2 is up to 1.18×10^{-1} in a mesh size of 15. For the present work, with the same mesh size and $M = 4$, the relative error L_2 is 1.70×10^{-2} for the FFSS plate, 3.36×10^{-2} for the FFSC plate, and 1.63×10^{-2} for the FFCC plate. These results indicate that the present method is about 10 times more accurate than the GDQ method for handling a free corner. Overall, the present method works very well for plates involving a free corner.

Table IX. Convergence of the FFFF plate.

M	L	N	Ω_1	Ω_2	Ω_3	Ω_4	Ω_5	L_2
2	6	7	8.632	17.203	20.565	22.502	35.474	2.41E-1
		9	11.574	19.564	24.175	33.361	34.771	6.56E-2
		11	12.240	19.585	24.165	34.563	34.867	4.09E-2
		13	13.080	19.595	24.119	34.547	36.270	2.33E-2
3	8	9	0.000	7.418	7.418	14.236	19.468	6.94E-1
		11	0.002	19.552	23.279	27.607	37.326	4.58E-1
		13	15.783	19.574	24.841	36.741	38.585	9.49E-2
		15	13.662	19.584	24.319	34.617	35.491	1.13E-2
4	9	11	0.000	19.604	27.209	30.625	30.625	4.57E-1
		13	16.885	19.601	25.222	37.724	38.772	1.31E-1
		15	14.571	19.599	24.406	35.488	35.761	3.97E-2
		17	13.505	19.597	24.335	34.361	34.943	6.19E-3
GDQ		15	10.303	19.596	22.146	30.026	30.803	1.38E-1
Reference [6]			13.468	19.596	24.271	34.801	34.801	
Reference [5]			13.489	19.789	24.432	35.024	35.024	

Table X. The numerical results obtained with adaptive grids ($N = 13, M = 5, L = 5$). The relative errors obtained with uniform grids are denoted as $L_{2,uni}$ and are listed for a comparison.

N	Ω_1	Ω_2	Ω_3	Ω_4	Ω_5	L_2	$L_{2,uni}$
SSSS	19.739	49.345	49.345	78.946	98.643	2.49E-4	2.13E-2
CCCC	35.985	73.386	73.394	108.253	131.424	7.65E-4	2.04E-2
FSSS	11.720	27.773	41.486	59.268	61.864	3.76E-3	9.81E-3
FCCC	24.322	40.066	64.639	76.583	81.332	1.04E-2	1.01E-2
FFSS	3.412	17.437	19.439	38.522	51.556	6.91E-3	1.19E-2
FFCC	6.953	23.786	26.869	47.434	63.384	6.96E-3	2.48E-2
FFSC	5.443	19.155	25.003	43.406	53.079	8.19E-3	3.87E-2
FFFS	6.681	15.012	25.611	26.160	49.243	5.82E-3	1.52E-2
FFFF	13.603	19.851	24.269	35.301	35.362	1.21E-2	2.33E-2

We next consider two plates that have more than one free corner. These cases are considerably more challenging. The convergence analysis of FFFS and FFFF plates is listed in Tables VIII and IX, respectively. For the FFFF plate, the results of Leissa and Narita [6] are used as the reference for computing the 'errors.' It is seen that the numerical results in both configurations have a similar level of accuracy compared with the configurations with only one free corner. For the GDQ method [25], the overall relative error L_2 is larger than 0.1 in these cases with a uniform mesh size of 15×15 . The relative GDQ error for a single mode is as large as 23.6 and the absolute error for a single mode is as large as 4.8. However, these errors are significantly reduced with a Chebyshev grid [25]. For the MIB method, the overall relative error L_2 is 1.73×10^{-2} for the FFFS plate and 3.97×10^{-2} for the FFFF plate. The relative MIB error for a single mode is less than 0.1 and the absolute error for a single mode is less than 1.0. The proposed MIB method works very well for multiple free edges and free corners. These results indicate the merits of using central FD schemes in vibration analysis.

It is worth mentioning that unlike energy-minimization-based methods, the proposed method does not use an energy minimization procedure. Therefore, the modal frequencies do not converge from above (or below). Consequently, mixed convergent behavior is observed. Nevertheless, the rate of convergence and accuracy of the present method are very satisfactory.

4.2. Non-uniform meshes

It is reported [25] that the GDQ method is very sensitive to the grid point distribution for plates with at least one free corner. Adaptive grids were proposed to stabilize the GDQ method. In this work, we are interested to know how the adaptive grids will improve the results of the proposed MIB method. Let us consider adaptive grids given by the Chebyshev coordinates:

$$X_i = \begin{cases} \frac{1}{2} \left[\cos \left(\frac{i-1}{N_x-1} \cdot \pi \right) - 1 \right], & 2L-2 \leq i \leq 0 \\ \frac{1}{2} \left[1 - \cos \left(\frac{i-1}{N_x-1} \cdot \pi \right) \right], & 1 \leq i \leq N_x \\ \frac{1}{2} \left[3 + \cos \left(\frac{i-1}{N_x-1} \cdot \pi \right) \right], & N_x+1 \leq i \leq N_x+2L-1 \end{cases} \quad (60)$$

$$Y_j = \begin{cases} \frac{1}{2} \left[\cos \left(\frac{j-1}{N_y-1} \cdot \pi \right) - 1 \right], & 2L-2 \leq j \leq 0 \\ \frac{1}{2} \left[1 - \cos \left(\frac{j-1}{N_y-1} \cdot \pi \right) \right], & 1 \leq j \leq N_y \\ \frac{1}{2} \left[3 + \cos \left(\frac{j-1}{N_y-1} \cdot \pi \right) \right], & N_y+1 \leq j \leq N_y+2L-1 \end{cases} \quad (61)$$

Non-uniform central FD weights are generated for this grid mesh by using the standard Lagrange polynomials [48].

Table X shows the numerical results of nine plate configurations under an adaptive mesh of 13×13 . As mentioned before, when N is small, a relatively small L produces better results than a relatively large L . Therefore, when $N = N_x = N_y = 13$, $L = 5$ is used in this study. It is known that when $L = 5$, $M = 2$ has the same order of accuracy as $M = 5$. The reason of using $M = 5$ here is to increase the stability of the method with the adaptive mesh. Comparing with the relative error L_2 obtained with the uniform mesh when $N = 13$ and $L = 6$, it is seen that although all the numerical results are slightly improved, the improvements on plate configurations involving at least one free corner are not as large as on those without free corners.

On uniform grids, the performance of the present MIB method is similar in all the configurations. In contrast, on adaptive grids, the accuracy decreases as the number of free edges increases in most cases. A possible reason is that for plates with simply supported and clamped edges, the boundary stress is a major source of numerical errors. Therefore, adaptive grids that provide more computational nodes near the edges increase the overall accuracy. However, for plates with at least one free corner, the errors induced by free motions cannot be simply suppressed by adaptive grids near the boundary.

4.3. Modal bending moments and shear forces

After decades efforts in structural analysis, a number of very reliable numerical methods, including the finite element method, have been developed to solve with desired accuracy for the global behavior of structures such as vibration frequency and buckling critical load. Nevertheless, to the best of our knowledge, no numerical methods are currently available to accurately predict the local aspects of stress resultants in specific cases, particularly, the stress resultants at a free boundary. All known finite element methods predict non-vanishing shearing forces at the free boundary,

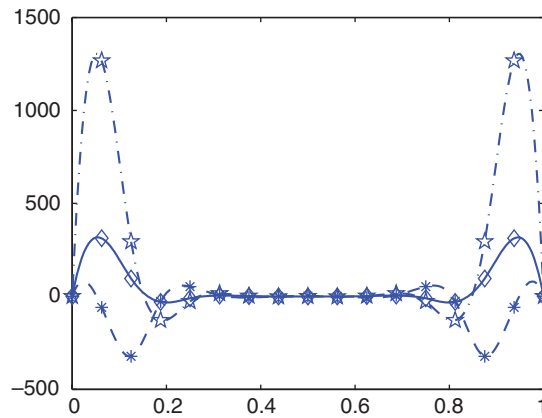


Figure 3. Modal bending moments *versus* the coordinate for the FFFF square plate vibrating in the first three modes. The modal bending moments are taken at $Y = \frac{5}{16}$. Solid line with diamonds, dashed line with stars, and dashed dotted line with pentastars are, respectively, for the first, second, and third modes.

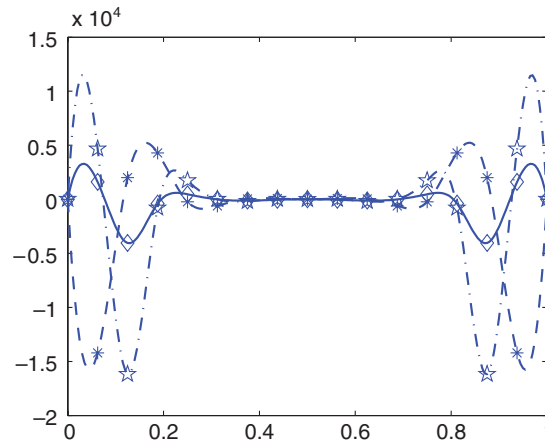


Figure 4. Modal shear forces *versus* the coordinate for the FFFF square plate vibrating in the first three modes. The modal shear forces are taken at $Y = \frac{5}{16}$. Solid line with diamonds, dashed line with stars, and dashed dotted line with pentastars are, respectively, for the first, second, and third modes.

which does not satisfy the free boundary condition. Therefore, it is very important to investigate whether the proposed MIB method provides vanishing modal bending moments and shear forces for free edges. To this end, we compute the modal bending moments and shear forces of the first three modes of the FFFF plate. Frequency parameters of these modes are listed in Table IX. The modal bending moments and shear forces are plotted in Figures 3 and 4, respectively, for the first three modes. Indeed, vanishing modal bending moments and shear forces are observed for all three modes examined. This comes with no surprise for the proposed MIB method, as it is designed to rigorously enforce all the boundary conditions. Specifically, the effort in the present work is given to ensure the implementation of the free edge boundary condition.

5. CONCLUDING REMARKS

The matched interface and boundary (MIB) method [41–44] is generalized for the free vibration analysis of rectangular plates. To test the performance of the present method, nine plates of simply supported, clamped, and free edges, and some of their important combinations are considered. To test the accuracy, first five eigenmodes are examined by relative L_2 errors. To test the convergence, mesh sizes of 9×9 , 11×11 , 13×13 , 15×15 , and 17×17 are employed. The number of layers of fictitious values, M , is selected in association with stencil width L . Different combinations of M , L , and N are studied in the convergence analysis. It is shown that the present method provides accurate and stable solutions for all nine plate configurations. As M , L , and N increase, the numerical solutions converge to the reference solutions provided by Leissa [5] or Leissa and Narita [6]. Comparison is made to the numerical results by the GDQ method [25]. As a global method, the GDQ performs better for plates without free corners. However, the proposed MIB method delivers much better results for plates with one or multiple free corners. A possible reason is that the GDQ method enforces the boundary conditions through one-sided discretizations, whereas the present method enforces the boundary conditions through symmetric discretizations. Moreover, the present method has a banded matrix.

It is well known that the performance of the GDQ method can be improved by using the so-called adaptive grids, which distribute dense grid nodes near the boundary. Such an approach provides results similar to those obtained by the present method with uniform grid. We have also implemented the MIB method with adaptive Chebyshev grids by using non-uniform central FD schemes. This study shows that the MIB method with adaptive grids reduces the errors of the SSSS and CCCC plates substantially. However, the improvement is not obvious for the remaining configurations that involve free edges or free corners.

The MIB method is a general approach for solving partial differential equations with material interfaces and/or special boundary conditions. The essential idea of the MIB method is to employ simple Cartesian grids to avoid grid generation even if the interface or the boundary is complex and irregular. The standard (higher-order) central FD schemes are utilized for the discretization of the governing equations in the entire domain, including the interface and boundary region. As the central FD schemes reach across the interface and/or the boundary, fictitious values are used to ensure that the numerical derivatives are locally computed on a ‘smooth function.’ Therefore, fictitious values are the smooth continuation of the original function across the interface and/or the boundary. This is the so-called domain extension. We make use of the interface and/or boundary conditions to determine the fictitious values, which, in turn, rigorously enforces the interface and/or boundary conditions. In order to construct higher-order schemes, the interface and/or boundary

conditions are repeatedly utilized. For elliptic equations, the domain is extended along one meshline at a time. Consequently, the 2D or 3D interface problem is locally reduced to 1D-like ones. However, due to the cross derivatives, the 2D domain extended has to be pursued simultaneously. It is possible to recast the present MIB scheme in terms of an interpolation formulation that bypasses the fictitious values or extended domains. It was shown that such an MIB approach is equivalent to the fictitious domain formulation [43].

A motivation of the present work is to deal with the difficulty of implementing free edge boundary conditions in our earlier discrete singular convolution (DSC) algorithm [28], which has been applied to a variety of vibration analysis of plates [29, 32–35]. The rigorous implementation of free edge boundary conditions is a pressing problem in structural analysis, as there is no general method available for the correct prediction of modal bending moments and shear forces at present. We have shown that for the proposed MIB method, the modal bending moments and shear forces indeed vanish at free edges. Furthermore, the ideas presented in the present MIB method can be easily used for the DSC algorithm to handle plates with free edges.

Another motivation of the present work is to study the possibility of generalizing the MIB method developed for elliptic equations with arbitrarily complex interfaces [45, 46, 49] to the structural analysis with similar geometric complexity. A relevant finding in the present work is that when $M=2$ and $N \geq 9$, the proposed method yields excellent results for all the plates examined. For arbitrarily complex geometries, $M=2$ is likely the best one can achieve, according to our experience in handling arbitrarily complex elliptic interface problems [45, 46, 49]. Therefore, the present results indicate a promise for this future generalization. This aspect is beyond the scope of this paper and is under our consideration.

ACKNOWLEDGEMENTS

This work was supported in part by NSF Grants DMS-0616704 and IIS-0430987. The authors thank Dr Shan Zhao for useful discussions.

REFERENCES

1. Chladni EFF. *Discoveries in the Theory of the Sound* (in German). Breitkopf und Hartel: Leipzig, 1787.
2. Cheung YK, Cheung MS. Flexural vibrations of rectangular and other polygonal plates. *Journal of the Engineering Mechanics Division (ASCE)* 1971; **97**:391–411.
3. Cheung MS. Finite strip analysis of structures. *Ph.D. Thesis*, University of Calgary, 1971.
4. Fan SC, Cheung YK. Flexural free vibrations of rectangular plates with complex support conditions. *Journal of Sound and Vibration* 1984; **93**:81–94.
5. Leissa AW. The free vibration of rectangular plates. *Journal of Sound and Vibration* 1973; **31**:257–293.
6. Leissa AW, Narita Y. Vibrations of completely free shallow shells of rectangular planform. *Journal of Sound and Vibration* 1984; **96**:207–218.
7. Warburton GB. The vibration of rectangular plates. *Proceedings of the Institution of Mechanical Engineers* 1954; **168**:371–384.
8. Chia CY. Non-linear vibration of anisotropic rectangular plates with non-uniform edge constraints. *Journal of Sound and Vibration* 1985; **101**:539–550.
9. Narita Y. Application of a series-type method to vibration of orthotropic rectangular plates with mixed boundary conditions. *Journal of Sound and Vibration* 1981; **77**:345–355.
10. Zitnan P. Vibration analysis of membranes and plates by a discrete least squares technique. *Journal of Sound and Vibration* 1996; **195**:595–605.
11. Donning BM, Liu WK. Meshless methods for shear-deformable beams and plates. *Computer Methods in Applied Mechanics and Engineering* 1998; **152**:47–71.

MATCHED INTERFACE AND BOUNDARY (MIB) METHOD

12. Lam KY, Liew KM, Chow ST. Free vibration analysis of isotropic and orthotropic triangular plates. *International Journal of Mechanical Sciences* 1990; **32**:455–464.
13. Liew KM, Lam KY. Application of two-dimensional orthogonal plate function to flexural vibration of skew plates. *Journal of Sound and Vibration* 1990; **139**:241–252.
14. Liew KM, Lam KY. A Rayleigh–Ritz approach to transverse vibration of isotropic and anisotropic trapezoidal plates using orthogonal plate functions. *International Journal of Solids and Structures* 1991; **27**:189–203.
15. Liew KM, Lam KY. On the use of 2-D orthogonal polynomials in the Rayleigh–Ritz method for flexural vibration of annular sector plates of arbitrary shape. *International Journal of Mechanical Sciences* 1993; **35**:129–139.
16. Young D. Vibration of rectangular plates by the Ritz method. *Transactions of the American Society of Mechanical Engineers, Journal of Applied Mechanics* 1950; **17**:448–453.
17. Lim CW, Liew KM. Vibrations of perforated plates with rounded corners. *Journal of Engineering Mechanics (ASCE)* 1995; **121**:203–213.
18. Zienkiewicz OC, Taylor RL. *The Finite Element Method*. McGraw-Hill: New York, 1989.
19. Leung AYT, Chan JKW. Fourier p-element for analysis of beams and plates. *Journal of Sound and Vibration* 1998; **212**:179–185.
20. Bellman R, Kashef BG, Casti J. Differential quadrature: a technique for the rapid solution of non-linear partial differential equations. *Journal of Computational Physics* 1972; **10**:40–52.
21. Bert CW, Jang SK, Striz AF. Two new approximate methods for analyzing free vibration of structural components. *American Institute of Aeronautics and Astronautics Journal* 1988; **26**:612–618.
22. Jang SK, Bert CW, Striz AG. Application of differential quadrature to static analysis of structural components. *International Journal for Numerical Methods in Engineering* 1989; **28**:561–577.
23. Shu C, Richards BE. Application of generalized differential quadrature method to structure problems. *International Journal for Numerical Methods in Fluids* 1992; **15**:791–798.
24. Du H, Lim MK, Lin RM. Application of generalized differential quadrature method to structure problems. *International Journal for Numerical Methods in Engineering* 1994; **37**:1881–1896.
25. Shu C, Du H. A generalized approach for implementing general boundary conditions in the GDQ free vibration analysis of plates. *International Journal of Solids and Structures* 1997; **34**:837–846.
26. Shu C, Wang CM. Treatment of mixed and non-uniform boundary condition in GDQ vibration analysis of rectangular plate. *Engineering Structures* 1999; **21**:125–134.
27. Xiang Y, Wang CM, Utsunomiya T, Machindamrong C. Benchmark stress-resultant distributions for vibrating rectangular plates with two opposite edges free. *Journal of Computational Structural Engineering* 2001; **1**:49–57.
28. Wei GW. Discrete singular convolution for the solution of the Fokker–Planck equations. *Journal of Chemical Physics* 1999; **110**:8930–8942.
29. Wei GW, Zhao YB, Xiang Y. Discrete singular convolution and its application to the analysis of plates with internal supports. I. Theory and algorithm. *International Journal for Numerical Methods in Engineering* 2002; **55**:913–946.
30. Hou YS, Wei GW, Xiang Y. DSC-Ritz method for the vibration analysis of Mindlin plates. *International Journal for Numerical Methods in Engineering* 2005; **62**:262–288.
31. Lim CW, Li ZR, Wei GW. DSC-Ritz method for the high frequency mode analysis of thick shallow shells. *International Journal for Numerical Methods in Engineering* 2005; **62**:205–232.
32. Wei GW. Vibration analysis by discrete singular convolution. *Journal of Sound and Vibration* 2001; **244**:535–553.
33. Wei GW, Zhao YB, Xiang Y. The determination of the natural frequencies of rectangular plates with mixed boundary conditions by discrete singular convolution. *International Journal of Mechanical Sciences* 2001; **43**:1731–1746.
34. Xiang Y, Zhao YB, Wei GW. Discrete singular convolution and its application to the analysis of plates with internal supports. II. Complex supports. *International Journal for Numerical Methods in Engineering* 2002; **55**:947–971.
35. Zhao YB, Wei GW. DSC analysis rectangular plates with nonuniform boundary conditions. *Journal of Sound and Vibration* 2002; **255**:203–225.
36. Wei GW, Zhao YB, Xiang Y. A novel approach for the analysis of high frequency vibrations. *Journal of Sound and Vibration* 2002; **257**:207–246.
37. Zhao YB, Wei GW, Xiang Y. Discrete singular convolution for the prediction of high frequency vibration of plates. *International Journal of Solids and Structures* 2002; **39**:65–88.
38. Civalek O. Numerical analysis of free vibrations of laminated composite conical and cylindrical shells: discrete singular convolution (DSC) approach. *Journal of Computational and Applied Mathematics* 2007; **205**:251–271.

39. Civalek O. Three-dimensional vibration, buckling and bending analyses of thick rectangular plates based on discrete singular convolution method. *International Journal of Mechanical Sciences* 2007; **49**:752–765.
40. Civalek O. The determination of frequencies of laminated conical shells via the discrete singular convolution method. *Journal of Mechanics of Materials and Structures* 2006; **1**:165–192.
41. Zhao S, Wei GW. High-order FDTD methods via derivative matching for Maxwell's equations with material interfaces. *Journal of Computational Physics* 2004; **200**:60–103.
42. Zhou YC, Zhao S, Feig M, Wei GW. High order matched interface and boundary (MIB) schemes for elliptic equations with discontinuous coefficients and singular sources. *Journal of Computational Physics* 2006; **213**:1–30.
43. Zhou YC, Wei GW. On the fictitious-domain and interpolation formulations of the matched interface and boundary (MIB) method. *Journal of Computational Physics* 2006; **219**:228–246.
44. Yu SN, Zhou YC, Wei GW. Matched interface and boundary (MIB) method for elliptic problems with sharp-edged interfaces. *Journal of Computational Physics* 2006; **224**:729–756.
45. Yu SN, Geng WH, Wei GW. Treatment of geometric singularities in the implicit solvent models. *Journal of Chemical Physics* 2006; **126**:244108.
46. Yu SN, Wei GW. Three dimensional matched interface and boundary (MIB) method for geometric singularities. *Journal of Computational Physics* 2007; **227**:602–632.
47. Zhao S, Wei GW, Xiang Y. DSC analysis of free-edged beams by an iteratively matched boundary method. *Journal of Sound and Vibration* 2005; **284**:487–493.
48. Fornberg B. Calculation of weights in finite difference formulas. *SIAM Review* 1998; **40**:685–691.
49. Geng WH, Yu SN, Wei GW. Treatment of charge singularities in implicit solvent models. *Journal of Chemical Physics* 2007; **127**:114106.